Published in final edited form as:
Magn Reson Med. 2012 August ; 68(2): 588–594. doi:10.1002/mrm.23250.

Chemical Exchange Saturation Transfer Magnetic Resonance Imaging of Human Knee Cartilage at 3 T and 7 T

Anup Singh, **Mohammad Haris**, **Kejia Cai**, **Victor B Kassey**, **Feliks Kogan**, **Damodar Reddy**, **Hari Hariharan**, and **Ravinder Reddy**
CMROI, Department of Radiology, University of Pennsylvania, Philadelphia, USA

Abstract

The sensitivity of chemical exchange saturation transfer (CEST) on glycosaminoglycans (GAG) in human knee cartilage (gagCEST) *in vivo* was evaluated at 3T and 7T field strengths. Calculated gagCEST values without accounting for B_0 inhomogeneity (~0.6 ppm) were > 20%. After B_0 inhomogeneity correction, calculated gagCEST values were negligible at 3T and ~6% at 7T. These results suggest that accurate B_0 correction is a pre-requisite for observing reliable gagCEST. Results obtained with varying saturation pulse durations and amplitudes as well as the consistency between numerical simulations and our experimental results indicate that the negligible gagCEST observed at 3T is due to direct saturation effects and fast exchange rate. Since GAG loss from cartilage is expected to result in a further reduction in gagCEST, gagCEST method is not expected to be clinically useful at 3T. At high fields such as 7T, this method holds promise as a viable clinical technique.

Keywords

MRI; CEST; saturation pulse; Cartilage; GAG; gagCEST

INTRODUCTION

Osteoarthritis (OA) is one of the debilitating joint diseases of the musculoskeletal system. It affects more than 10% of adults and 70% of the population over the age of 65 years and has a significant negative impact on the quality of life of elderly individuals (1–3). While OA is now increasingly viewed as a metabolically active joint disorder of diverse etiologies, cartilage tissue degeneration is primarily implicated. It is generally believed that the initiating event of OA is predominantly due to loss of proteoglycans from the tissue (4). Proteoglycans (PG) are complex macromolecules that consist of proteins and polysaccharides. Aggrecan is the most common of these PG, and accounts for ~80–90% of the total PG. It consists of a protein core with a long extended domain to which many glycosaminoglycan (GAG) side chains are attached. Chondroitin sulfate (CS) is the predominant GAG molecule found in cartilage. In order for appropriate therapeutic

Address for Correspondence. Anup Singh, PhD, Center for Magnetic Resonance and Optical Imaging (CMROI), Department of Radiology, University of Pennsylvania, B1 Stellar-Chance Laboratories, 422 Curie Boulevard, Philadelphia, PA 19104-6100, Tel: (215) 898-9357, Fax: (215) 573-2113, anups.minhas@gmail.com.

intervention in OA, there is a critical need for diagnostic methods that quantify the early molecular changes in cartilage before the manifestation of morphological changes.

Since conventional magnetic resonance imaging (MRI) is neither proven sensitive nor accurate for the detection of early biochemical changes associated with the loss of PG, there have been several sophisticated MRI methods proposed to quantify these changes *in vivo*. These include sodium MRI, T1rho ($T_{1\rho}$) MRI and delayed Gadolinium enhanced MRI contrast (dGEMRIC) (5–7). While sodium MRI is highly specific to PG, it requires special coils and hardware (multi-nuclear option). It is also associated with low SNR and requires ultrahigh fields. dGEMRIC on the other hand is a promising method that can be performed on standard clinical scanners. However, it has logistical issues such as long waiting periods following the injection of contrast agent. $T_{1\rho}$ MRI is a novel imaging method that has the ability to generate endogenous contrast that is sensitive to *in vivo* PG and collagen content(6). Recently, it has been shown that chemical exchange saturation transfer (CEST) of labile –OH protons on GAG with bulk water leads to a significant reduction of bulk water magnetization creating "gagCEST" (8). Using this approach significant gagCEST was reported from both *ex vivo* and *in vivo* cartilage without any systematic analysis of static magnetic field (B_0) inhomogeneity (8).

It is well known that the B_0 inhomogeneity would significantly affect the accuracy of the computed CEST values (9–11). B_0 correction requires an estimate of local B_0 variation. For B_0 estimation, one can either use gradient echo MRI methods (12) or off-resonance saturation based methods (10,11,13). Recently published water saturation shift referencing (WASSR) approach (10) is also an off resonance saturation based method with optimized saturation pulses to provide only direct water saturation. For B_0 correction, one can use either analytical expression in steady state saturation conditions (9) or interpolated (or fitted) z-spectral data (10,11,13). We have used interpolated WASSR data for B_0 estimation.

In the current study, the feasibility of performing gagCEST on human cartilage *in vivo* was evaluated at 3T and 7T field strengths. Human cartilage gagCEST maps were computed before and after the correction of B_0 inhomogeneity. Saturation pulse parameters were optimized to obtain maximal gagCEST in human cartilage and numerical simulations were performed to examine the effects of direct saturation (14) of water as well GAG –OH protons on the observed gagCEST.

MATERIALS AND METHODS

Theoretical

In CEST experiments, frequency selective saturation of solute spins that are in exchange with solvent spins (e.g., water) leads to the transfer of saturated magnetization to the solvent thus decreasing the signal intensity of the solvent spins. Subsequently, longitudinal relaxation returns each nuclear spin system to its equilibrium values and eventually the system reaches a steady state. The steady state magnetization is given as:

$$\frac{M_{sat\infty}}{M_0} = \frac{1}{1+k_1 T_{1w}} \quad [1]$$

where $M_{sat\infty}$ is the steady-state amplitude of the water proton magnetization during the irradiation of exchangeable solute spins; M_0 is the amplitude of the water proton magnetization in the absence of saturation, k_1 is the pseudo first order exchange rate constant, and T_{1w} is the longitudinal relaxation time of water protons (14–16). This magnetization is then imaged to detect the CEST effect from solute nuclear spins. In order for the CEST effect to be efficiently observed, the slow to intermediate exchange condition ($\Delta\omega > k$) must be fulfilled where $\Delta\omega$ is the chemical shift (or offset frequency) of the exchanging spins and k is the exchange rate. In general the CEST effect of the solute spins is computed using following equation:

$$CEST_{asym}(\Delta\omega) = \frac{M_{sat}(-\Delta\omega) - M_{sat}(\Delta\omega)}{M_0} \quad [2]$$

where M_0 is the water equilibrium magnetization, M_{sai} ($\pm\Delta\omega$) are the water magnetizations obtained with saturation at a '+' or '−' $\Delta\omega$ offset of the water resonance. In interpreting the CEST effect, other factors that play role are the amplitude and duration of the saturation pulse. These effects can be incorporated into a general solution obtainable from a theoretical analysis of a two-site exchange model in the presence of solute saturation. An analytical expression for the CEST effect can be derived (17–20) as:

$$CEST_{asym}(\Delta\omega) = \frac{k\alpha f}{R_{1w} + kf}[1 - e^{-(R_{1w}+kf)t_{sat}}] \quad [3]$$

where k is exchange rate (s^{-1} or Hz), α is an efficiency factor with $\alpha = 1$ describing complete saturation (obtained with a sufficiently high amplitude saturation pulse), f is the fraction of exchangeable protons with respect to the total number of protons including water, R_{1w} ($=1/T_{1w}$) is the longitudinal relaxation rate of water protons and t_{sat} is the length of the saturation pulse.

While Eq. [3] is useful in understanding the general CEST principles, its applicability is limited to solute selective steady state saturation only at $+\Delta\omega$ offset frequency with no other saturation contaminations. In practice there is contamination from the DS of water to both M_{sat} ($\pm\Delta\omega$) and from DS of solute protons while saturating at $-\Delta\omega$ to M_{sat} ($-\Delta\omega$). DS of water reduces the available bulk water protons for chemical exchange and reduces CEST contrast. DS of solute protons while saturating at $-\Delta\omega$ additionally reduces water magnetization due to chemical exchange with the solute protons. In such cases to fully understand CEST and DS effects, one needs to resort to numerical simulations of Bloch-McConnell equations (17).

The effects of B_0 and B_1 variations on the observed CEST values are rather complex. Since the CEST asymmetry is based on the subtraction of images M_{sat} ($\pm\Delta\omega$), any asymmetry created with local B_0 variation will contaminate the observed CEST asymmetry. Hence, a very good estimate and correction of local B_0 inhomogeneity is imperative to get accurate CEST asymmetry. B_1 variations affect both the CEST effect (Eq. [3] provides a hint for this through the empirical factor α) as well as the amount of DS contamination.

CEST MR Sequence

The pulse sequence used in current study consists of a frequency selective saturation pulse train (user selected saturation offset frequency ($\Delta\omega$), saturation duration and B_{1rms}) followed by a chemical shift selective fat saturation pulse and a segmented RF spoiled gradient echo (GRE) readout acquisition with centric phase encoding order. At the end of the GRE acquisition segments, a variable delay has been added to provide T1 recovery and keep the sequence under system RF safety limits. This sequence is flexible enough to be used for both the WASSR data acquisition as well as CEST imaging.

The saturation pulse train is composed of Hanning windowed rectangular pulses and delays between them. At 3T a 48 ms pulse with a 2 ms delay is used where as at 7T a 99.8 ms pulse with a 0.2 ms delay is used. The number of pulses in the train can be adjusted to provide variable saturation duration. The Hanning window shape and pulse duration were chosen based on MRI scanner hardware limits and minimal artifacts in phantom tests. The peak B_1 of the Hanning windowed pulse is set to provide the required B_{1rms} value. The saturation pulse excitation bandwidth (50%) is 10 Hz with a 1% bandwidth of 40 Hz (~0.28 ppm at 3T) for saturation train duration of 0.5 s. For longer saturation durations, these bandwidths are narrower.

Human Studies

The study was conducted under an approved Institutional Review Board protocol of the University of Pennsylvania. Five subjects were taken from a normal population in the age range of 28–40 yrs. Informed consent from each volunteer was obtained after explaining the study protocol. CEST imaging and z-spectrum acquisitions on the human knee were performed at 3T using an 18 cm diameter, eight-channel transmit–receive phased-array (PA) knee coil on a Siemens clinical scanner (Magnetom Tim Trio, Siemens Medical Solutions, Malvern, PA) and at 7T using the standard circularly polarized (CP) head coil on a Siemens 7T research scanner (Siemens Medical Solutions, Malvern, PA).

The actual study protocol consisted of the following steps: a localizer, WASSR, z-spectral or CEST acquisitions and B_1 data collection. For WASSR acquisitions, $\Delta\omega$ range of −1 to +1 ppm with step size of 0.05 ppm was used. For z-spectrum acquisitions, $\Delta\omega$ range of −5 to +5 ppm with step size of 0.1 ppm was used. For CEST acquisitions, a limited $\Delta\omega$ range required for B_0 correction was used. This range was based on a quick inspection of dark regions in raw WASSR images (on scanner) at different WASSR saturation $\Delta\omega$. Typical $\Delta\omega$ ranges used for CEST acquisitions were −1.7 ppm to −0.3 ppm and 0.3 ppm to 1.7 ppm with 0.1 ppm steps for a total of 30 images.

Knee imaging parameters were: slice thickness = 5 mm, flip angle = 10°, readout TR = 5.6 ms, TE = 2.7 ms, field of view = 140×140 mm^2, matrix size = 192×192 with a segment size of 96. The whole sequence was repeated every 6 s at 3T and every 8 s at 7T for each $\Delta\omega$.

For WASSR acquisitions, a 0.2 s saturation pulse with B_{1rms} of 0.13 μT was used in all cases. For complete z-spectral acquisitions, a 0.5 s saturation pulse with a B_{1rms} of 2.2 μT was used with the same volunteer (n = 2) at 3T and 7T. For investigating the effects of saturation parameters, multiple CEST images were collected on two volunteers at both 3T

and 7T using saturation pulses with B_{1rms} of 18.5 Hz (0.4 μT) and 31 Hz (0.7 μT) over a duration range of 0.1–2.0 s, 62 Hz (1.4 μT) and 93 Hz (2.2 μT) over a duration range of 0.1 – 1.0 s and 124 Hz (2.9 μT) over a duration range of 0.1–0.5 s. At higher B_{1rms} values, the signal to noise ratios of CEST images using longer duration pulses were too poor to measure reliable gagCEST.

CEST imaging was performed with 4 volunteers on both 3T and 7T using the imaging protocol as described above with a saturation duration of 0.5 s and B_{1rms} of 2.2 μT.

Data analysis

All image processing and data analysis was performed using in-house programs written in MATLAB (version 7.5, R2007b). The cartilage section was manually segmented from the anatomical image and all data processing was performed only on this section. Acquired CEST data (at $\Delta\omega = \pm 1.0$ ppm) or z-spectral data (typically −5.0 to +5.0 ppm) were directly used to generate gagCEST maps or z-spectral asymmetry curves using Eq. [2] to get data without B_0 correction. The mean and standard deviation of gagCEST or CEST asymmetry values were calculated over the small region of interest (ROI) drawn on cartilage region in the image. The gagCEST map was overlaid on one of the original anatomical images.

B_0 and B_1 Corrections

WASSR data acquired over the Δω range of + 1.0 to −1.0 ppm at steps of 0.05 ppm at each voxel are smoothed and interpolated using a cubic spline to generate data with a step size of 0.01 ppm. The Δω corresponding to the minimum of the interpolated data was used as the B_0 value (δω) at each voxel (resolution = 0.01 ppm). Acquired CEST data (at offset frequencies, typically +0.3 to +1.7 ppm and −0.3 to −1.7 ppm) or z-spectral data (typically −5.0 to +5.0 ppm) were smoothed and interpolated using a cubic spline to generate data with a step size of 0.01 ppm. For B_0 inhomogeneity correction, each voxel data value at Δω ppm was replaced by the interpolated data value from (Δω –δω) ppm. Either z-spectral asymmetry curves or CEST maps (based on the data from ±1.0 ppm) were generated using Eq. [2].

B_1 field maps were obtained using a 2D single slice fast spin echo readout sequence with TE = 12 ms TR = 6 s, 128 × 128 image matrix. Two images were obtained using preparation square pulses with flip angles 30° and 60° (pulse duration = 0.3 ms). The 30° flip angle RF pulse amplitude was used as the reference B_1 or B_{1ref}. Flip angle (θ) maps were generated by solving following equation:

$$\frac{\cos(2\theta)}{\cos(\theta)} = \frac{S(2\theta)}{S(\theta)} \quad [4]$$

where $S(\theta)$ and $S(2\theta)$ denote voxel signals in an image with a preparation flip angle of θ and 2θ respectively. From the flip angle map, a B_1 field map can be obtained using the relation, $B_1 = \theta/(360\tau)$. The coefficient B_1/B_{1ref} can be used if needed for B_1 scaling of CEST values (21).

Simulations

Bloch McConnell equation solvers with two exchanging components (water and GAG) were written in MATLAB for analyzing the effects of CEST and DS at both 3T and 7T with the saturation pulse trains used in the experiments (14). Both the residual water magnetization affected only by DS without any CEST effects as well as the CEST asymmetry values contaminated with DS at different offset frequencies were calculated for the different saturation pulse durations and B_{1rms} values used in the experiments.

RESULTS

Figure 1 shows Z-spectra (a, c) and CEST asymmetry (b, d) plots of a small ROI from human knee cartilage before and after B_0 inhomogeneity corrections from 3T and 7T. Without any corrections for B_0 inhomogeneity, a clear shift (~0.6 ppm) in the Z-spectrum was observed in this ROI. This shift in the data is removed after correction for the B_0 inhomogeneity. gagCEST calculated from the asymmetry plots generated without B_0 correction show large effects (>20%) while after B_0 correction the calculated gagCEST was negligible at 3T and ~6% at 7T. The error bars shown in figure 1 represent the standard deviation of the gagCEST values at each ppm over the ROI. A large number of voxels in corrected gagCEST map at 3T showed both positive and negative values at different $\Delta\omega$. Hence the gagCEST asymmetry derived through integration over an offset range around 1 ppm is also negligible. The effect of B_1 inhomogeneity in the cartilage region was minor (<10%) in the current study at both 3T and 7T and hence no correction was necessary.

The top row of figure 2 shows a fat suppressed anatomical human knee image (a) and gagCEST maps (b, c) without and with B_0 correction at 3T. Without any correction for B_0 inhomogeneity, a >20% gagCEST was observed in cartilage (Fig. 2b). With B_0 inhomogeneity corrections negligible gagCEST was observed. The corresponding images and maps from the same volunteer at 7T are shown in bottom row. After B_0 correction ~6% gagCEST was observed.

Figure 3 shows plots of knee cartilage gagCEST at varying saturation B_{1rms} and durations obtained at both 3T (a) and 7T (b). Observed gagCEST was negligible at 3T for all B_{1rms} and durations while at 7T the maximum gagCEST was observed at saturation B_{1rms} of 2.2 μT and duration of 0.5 s.

Figure 4 depicts corrected gagCEST images from the 4 healthy volunteers at 3T (a) and 7T (b). Again, the observed gagCEST at 3T is negligible while at 7T it is ~6%.

Figure 5 shows our simulation results at 3T and 7T: (a) the effect of water DS for a 0.5 s duration saturation pulse at different B_{1rms} values. (b) The effect of DS of the GAG pool while saturating at −1 ppm for a 0.5 s duration saturation pulse at various B_{1rms} values. The reductions in water and GAG magnetizations reduce the gagCEST sensitivity at 3T. (c) Simulated CEST asymmetry spectra for a saturation B_{1rms} of 2.2 μT and duration of 0.5 s show that the theoretical gagCEST expected at 3T is 0.5% at 1.0 ppm while at 7T it is 5.8%. This is in line with the experimental results reported above.

DISCUSSION

Given the geometry of knee and cartilage distribution, as shown in this study, there may be substantial B_0 field variations within and around the cartilage. B_0 inhomogeneity leads to a shift in the z-spectra and affects the magnitude of gagCEST observed at 1.0 ppm (Fig.1). This suggests that the significant gagCEST (>20%) reported earlier at 3T (8) is mainly due to the presence of B_0 field inhomogeneity in the human cartilage. After B_0 corrections, calculated gagCEST values were negligible at 3T and ~6% at 7T (Fig 2 & Fig. 4).

The saturation pulse amplitude (B_1) dependency of gagCEST has been evaluated in *in vivo* cartilage (Fig. 3). These experimental results show that gagCEST stayed negligible when B_{1rms} was varied between 0.4 to 2.9 μT at 3T and peaks at saturation B_{1rms} of ~2.2 μT and duration of ~0.5 s with a value of ~6%. It is interesting to note that at lower B_{1rms} values, we seem to be getting a small negative gagCEST. This is consistent with a nuclear Overhauser effect (NOE) induced water signal loss from GAG CH protons while saturating at −1.0 ppm. At higher B_{1rms} values, this effect is suppressed. This has also been previously shown with *in vitro* data (8).

As seen from our simulation results (Fig. 5), one of the main reasons for the reduced efficiency of gagCEST at 3T seems to be DS effects leading to reduced water magnetization (when saturating at (±1 ppm) as well as chemical exchange with the reduced GAG magnetization when saturating at (−1 ppm). Another potential major cause for the gagCEST efficiency difference between 3T and 7T is that the reported –OH protons exchange rate k_{ex} of 1000 s^{-1} (22) is in fast exchange regime at 3T ($k_{ex} > \Delta\omega$ (~800rad s^{-1})) whereas it is in slow exchange regime at 7T ($k_{ex} <\sim \Delta\omega$(~1800 rad s^{-1})).

It is worthwhile to report the recent gagCEST study (23) in human knee cartilage performed at 7T has shown a peak value ~3% at 1.2 ppm. Since there is not enough information about the experimental parameters used in this study, it is difficult to compare our results with this study.

In summary, numerical simulations as well experimental results demonstrate that the DS effects of water and GAG are substantial contributors for negligible gagCEST observed after B_0 correction in cartilage at 3T. Since GAG loss from cartilage is expected to result in a further reduction in gagCEST, this method is not expected to lead to accurate quantification of GAG content in healthy or degenerated cartilage at 3T. Given its magnitude (~6%) gagCEST at high fields such as 7T holds promise as a clinically viable technique.

Acknowledgments

This work was performed at an NIH-NCRR supported Biomedical Technology Research Center (P41RR002305) and was supported by NIAMS grant NIH-R01AR45404.

REFERENCES

1. Peat G, McCarney R, Croft P. Knee pain and osteoarthritis in older adults: a review of community burden and current use of primary health care. Ann Rheum Dis. 2001; 60(2):91–97. [PubMed: 11156538]

2. Arden N, Nevitt MC. Osteoarthritis: epidemiology. Best Pract Res Clin Rheumatol. 2006; 20(1):3–25. [PubMed: 16483904]
3. Garstang SV, Stitik TP. Osteoarthritis: epidemiology, risk factors, and pathophysiology. Am J Phys Med Rehabil. 2006; 85(11 Suppl):S2–S11. quiz S12–14. [PubMed: 17079976]
4. Malemud CJ. Changes in proteoglycans in osteoarthritis: biochemistry, ultrastructure and biosynthetic processing. J Rheumatol Suppl. 1991; 27:60–62. [PubMed: 2027133]
5. Reddy R, Insko EK, Noyszewski EA, Dandora R, Kneeland JB, Leigh JS. Sodium MRI of human articular cartilage in vivo. Magn Reson Med. 1998; 39(5):697–701. [PubMed: 9581599]
6. Regatte RR, Akella SV, Lonner JH, Kneeland JB, Reddy R. T1rho relaxation mapping in human osteoarthritis (OA) cartilage: comparison of T1rho with T2. J Magn Reson Imaging. 2006; 23(4): 547–553. [PubMed: 16523468]
7. Tiderius CJ, Olsson LE, Leander P, Ekberg O, Dahlberg L. Delayed gadolinium-enhanced MRI of cartilage (dGEMRIC) in early knee osteoarthritis. Magn Reson Med. 2003; 49(3):488–492. [PubMed: 12594751]
8. Ling W, Regatte RR, Navon G, Jerschow A. Assessment of glycosaminoglycan concentration in vivo by chemical exchange-dependent saturation transfer (gagCEST). Proc Natl Acad Sci U S A. 2008; 105(7):2266–2270. [PubMed: 18268341]
9. Sun PZ, Farrar CT, Sorensen AG. Correction for artifacts induced by B-0 and B-1 field inhomogeneities in pH-Sensitive chemical exchange saturation transfer (CEST) Imaging. Magnetic Resonance in Medicine. 2007; 58(6):1207–1215. [PubMed: 17969015]
10. Kim M, Gillen J, Landman BA, Zhou J, van Zijl PC. Water saturation shift referencing (WASSR) for chemical exchange saturation transfer (CEST) experiments. Magn Reson Med. 2009; 61(6): 1441–1450. [PubMed: 19358232]
11. Stancanello J, Terreno E, Castelli DD, Cabella C, Uggeri F, Aime S. Development and validation of a smoothing-splines-based correction method for improving the analysis of CEST-MR images. Contrast Media Mol I. 2008; 3(4):136–149.
12. Webb P, Spielman D, Macovski A. Inhomogeneity Correction for Invivo Spectroscopy by High-Resolution Water Referencing. Magnetic Resonance in Medicine. 1992; 23(1):1–11. [PubMed: 1734171]
13. Zhou J, Payen JF, Wilson DA, Traystman RJ, van Zijl PC. Using the amide proton signals of intracellular proteins and peptides to detect pH effects in MRI. Nat Med. 2003; 9(8):1085–1090. [PubMed: 12872167]
14. Sherry AD, Woods M. Chemical exchange saturation transfer contrast agents for magnetic resonance imaging. Annu Rev Biomed Eng. 2008; 10:391–411. [PubMed: 18647117]
15. Ward KM, Aletras AH, Balaban RS. A new class of contrast agents for MRI based on proton chemical exchange dependent saturation transfer (CEST). J Magn Reson. 2000; 143(1):79–87. [PubMed: 10698648]
16. Ward KM, Balaban RS. Determination of pH using water protons and chemical exchange dependent saturation transfer (CEST). Magn Reson Med. 2000; 44(5):799–802. [PubMed: 11064415]
17. Woessner DE, Zhang S, Merritt ME, Sherry AD. Numerical solution of the Bloch equations provides insights into the optimum design of PARACEST agents for MRI. Magn Reson Med. 2005; 53(4):790–799. [PubMed: 15799055]
18. van Zijl PC, Jones CK, Ren J, Malloy CR, Sherry AD. MRI detection of glycogen in vivo by using chemical exchange saturation transfer imaging (glycoCEST). Proc Natl Acad Sci U S A. 2007; 104(11):4359–4364. [PubMed: 17360529]
19. McMahon MT, Gilad AA, Zhou J, Sun PZ, Bulte JW, van Zijl PC. Quantifying exchange rates in chemical exchange saturation transfer agents using the saturation time and saturation power dependencies of the magnetization transfer effect on the magnetic resonance imaging signal (QUEST and QUESP): Ph calibration for poly-L-lysine and a starburst dendrimer. Magn Reson Med. 2006; 55(4):836–847. [PubMed: 16506187]
20. Zhou J, Wilson DA, Sun PZ, Klaus JA, Van Zijl PC. Quantitative description of proton exchange processes between water and endogenous and exogenous agents for WEX, CEST, and APT experiments. Magn Reson Med. 2004; 51(5):945–952. [PubMed: 15122676]

21. Haris M, Cai K, Singh A, Hariharan H, Reddy R. In vivo mapping of brain myo-inositol. Neuroimage. 2011; 54(3):2079–2085. [PubMed: 20951217]

22. Hills BP, Cano C, Belton PS. Proton Nmr Relaxation Studies of Aqueous Polysaccharide Systems. Macromolecules. 1991; 24(10):2944–2950.

23. Schmitt B, Zbyn S, Stelzeneder D, Jellus V, Paul D, Lauer L, Bachert P, Trattnig S. Cartilage Quality Assessment by Using Glycosaminoglycan Chemical Exchange Saturation Transfer and (23)Na MR Imaging at 7 T. Radiology. 2011; 260(1):257–264. [PubMed: 21460030]

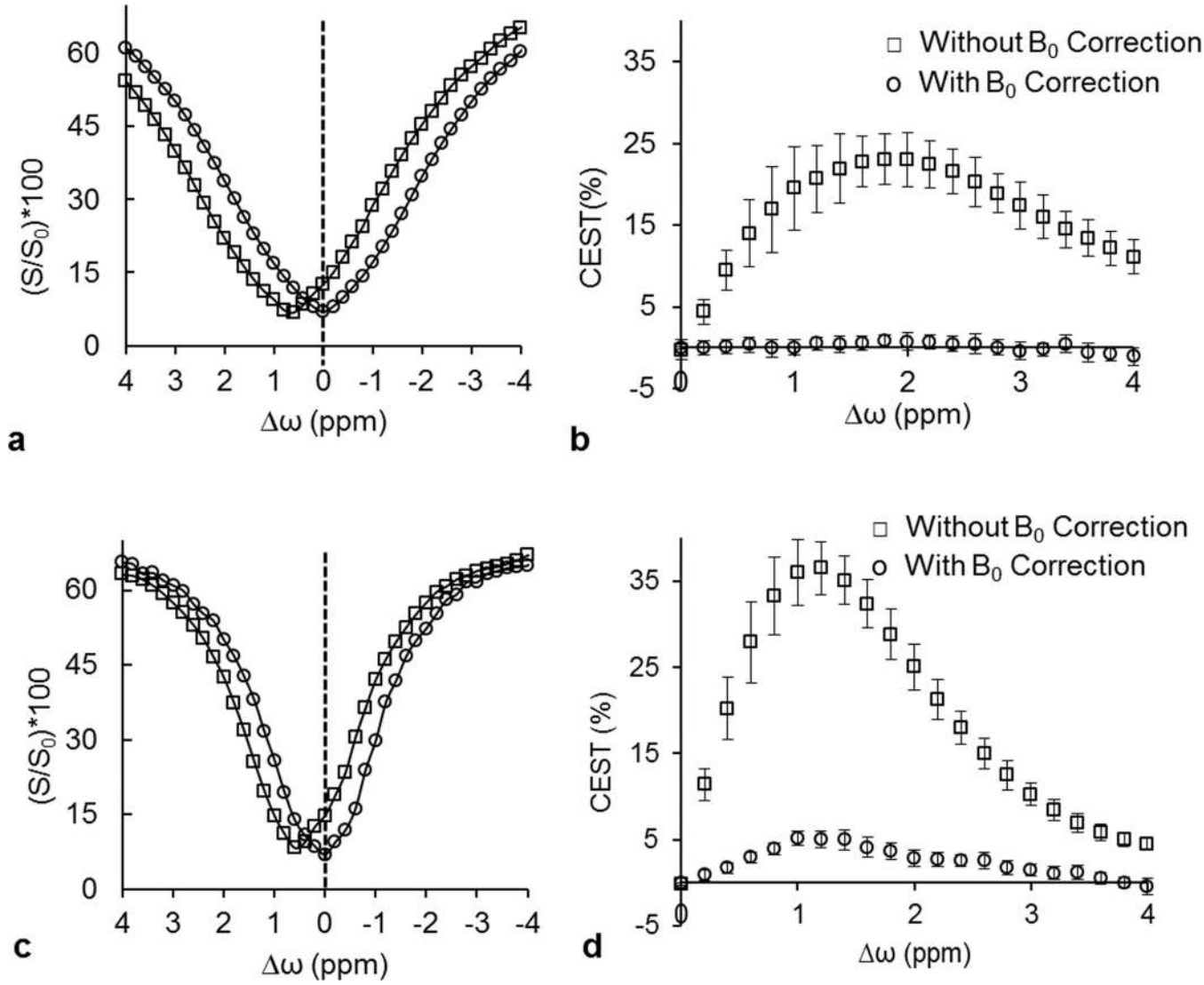

Figure 1.

Z-spectra (a, c) and $CEST_{asym}$ plots (b, d) of human knee cartilage without (□) and with (○) B_0 inhomogeneity correction obtained at 3T and 7T respectively. Saturation pulse parameters were B_{1rms} of 2.2 μT and duration of 0.5 s.

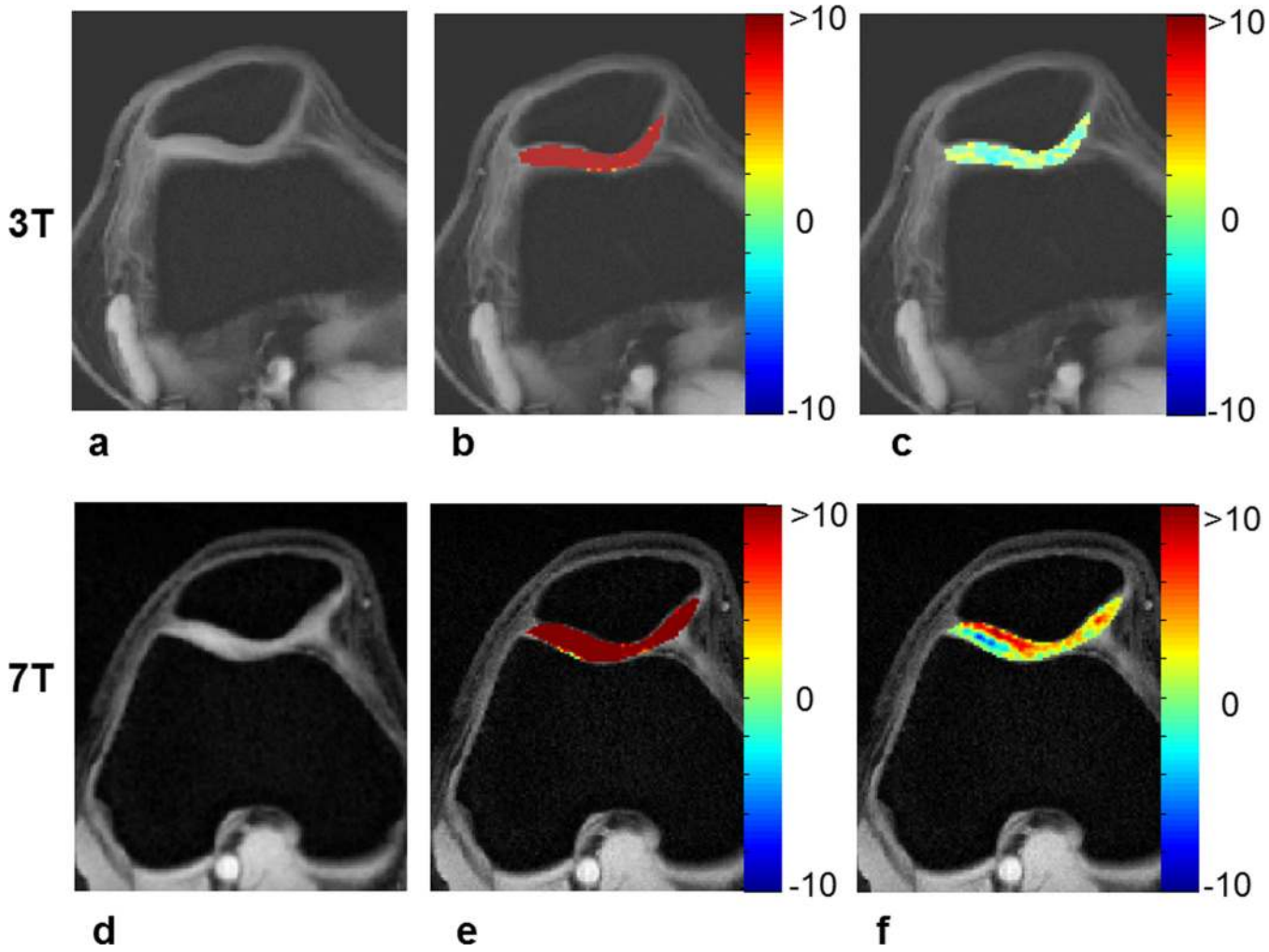

Figure 2.

Top row contains fat suppressed anatomical image from knee cartilage (a), gagCEST maps of cartilage obtained without (b) and with correction (c) for B_0 inhomogeneity at 3T. Corresponding images and maps from 7T are shown in the bottom row. Saturation pulse parameters were B_{1rms} of 2.2 μT and duration of 0.5 s.

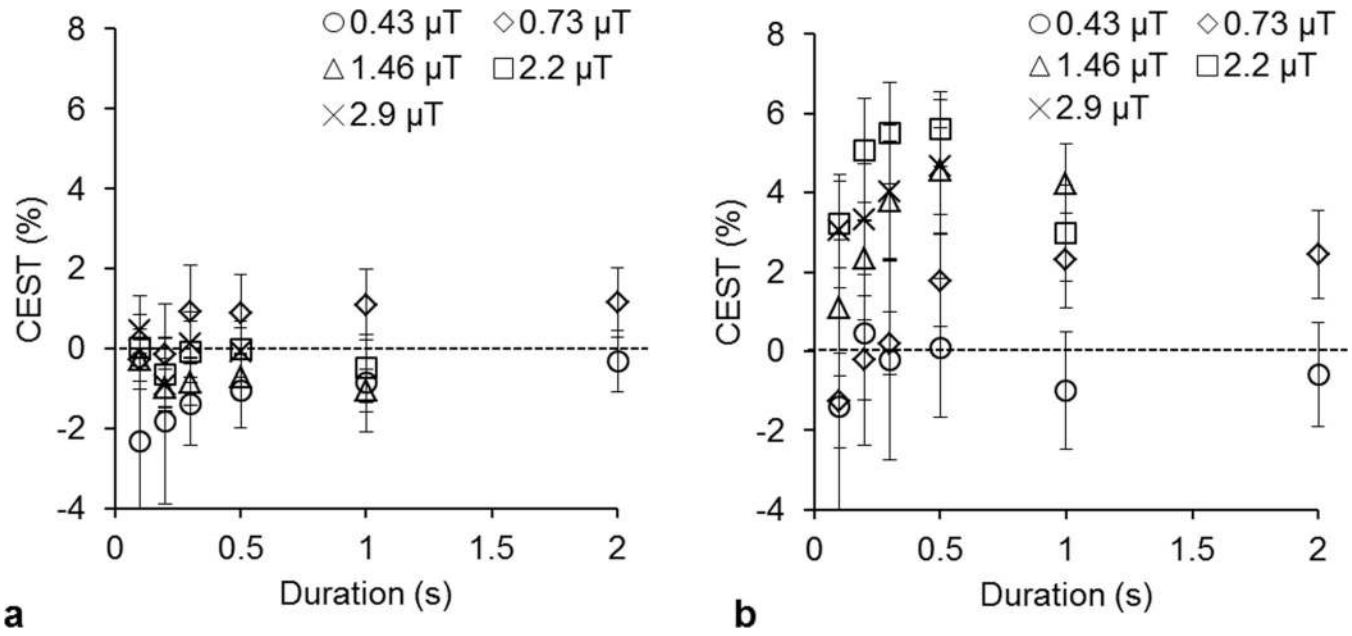

Figure 3.

The saturation B_{1rms} and duration dependence of gagCEST from human knee cartilage at 3T (a) and 7T (b). Different B_{1rms} employed were: 0.43 μT(○), 0.73 μT(◊), 1.46 μT(Δ), 2.2 μT(□), and 2.9 μT(x).

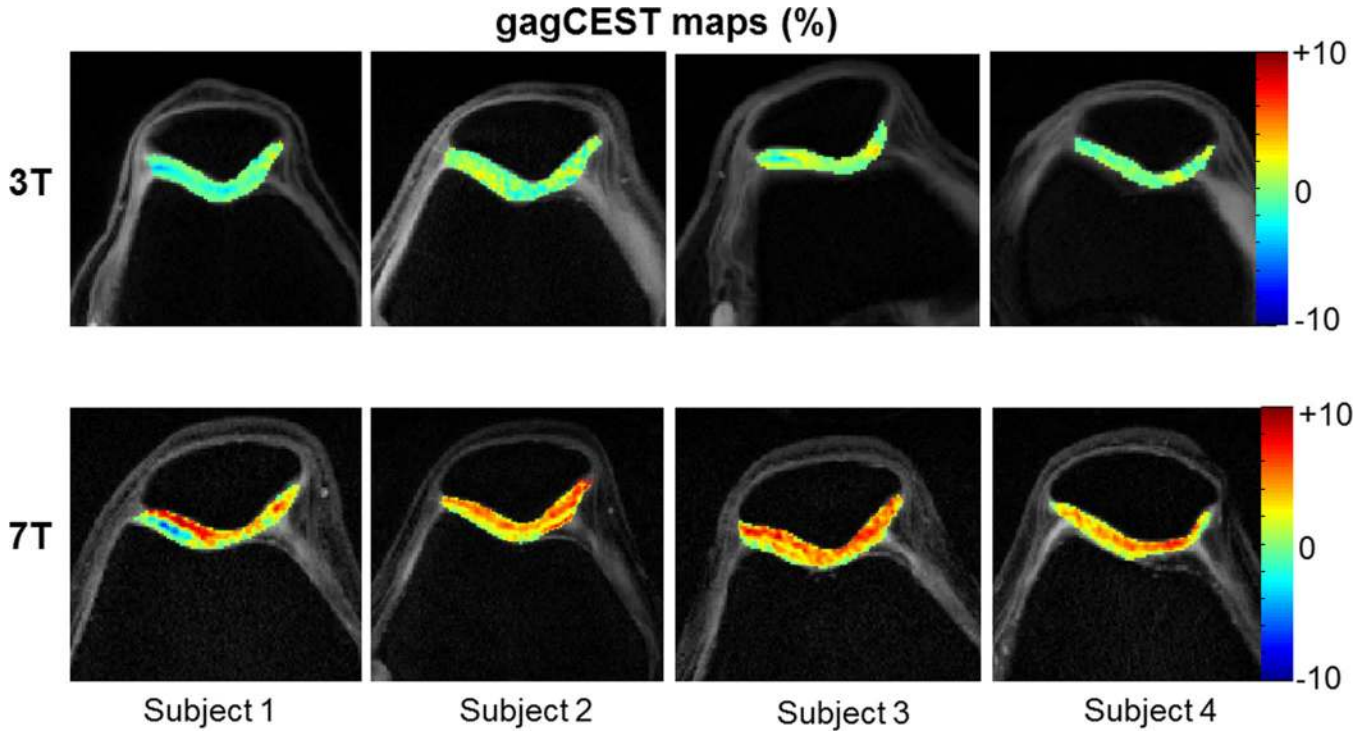

Figure 4.

Corrected knee gagCEST maps from the 4 volunteers at 3T (top row) and 7T (bottom row) for a saturation B_{1rms} of 2.2 μT and duration of 0.5 s.

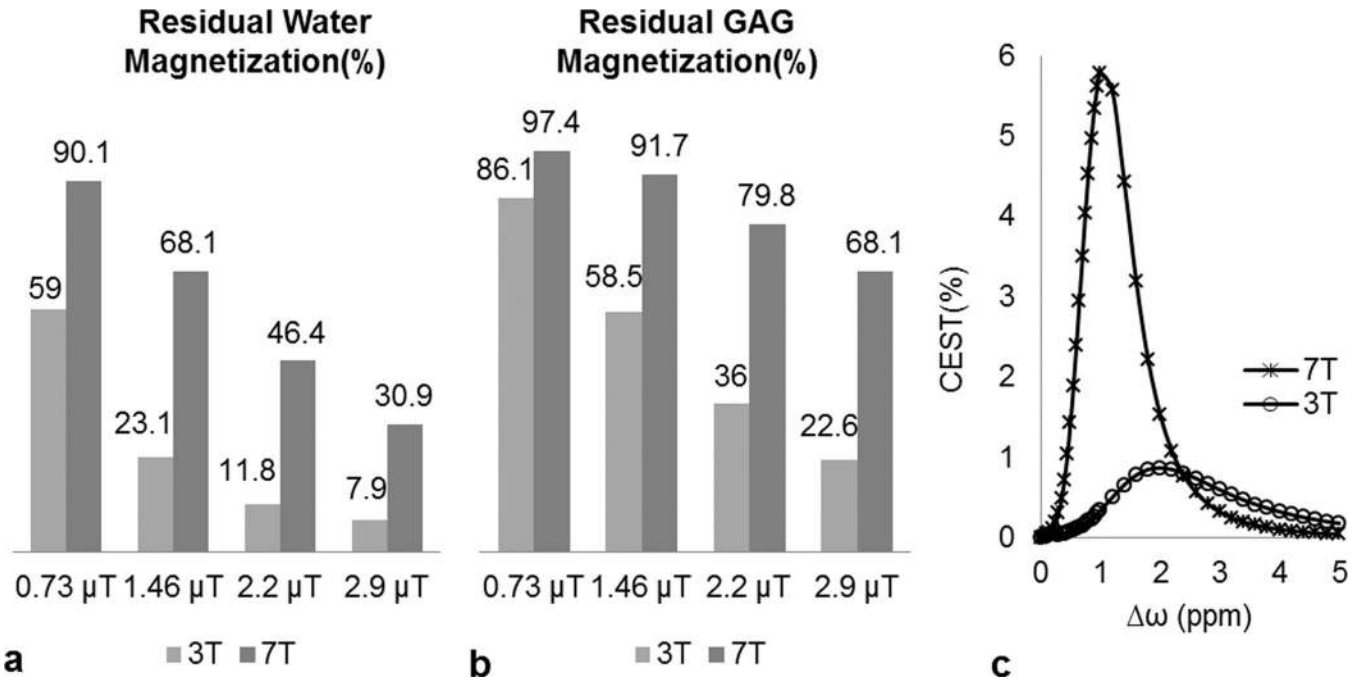

Figure 5.

Simulation results. (a) Residual water magnetization (%) after a 0.5 s duration saturation pulse train with different B_{1rms} values applied at a 1 ppm offset symmetrically around water at 3T and 7T. (b) Residual GAG magnetization (%) after a 0.5 s duration saturation pulse train with different B_{1rms} values applied at a −1 ppm offset from water at 3T and 7T. (c) gagCEST asymmetry plot simulations at 3T and 7T for a 0.5 s duration saturation pulse train with B_{1rms} = 2.2 μT. Other simulation parameters: for water, concentration = 88 M (80% water fraction in cartilage), T1 = 1.2 s at 3T and 1.5 s at 7T, T2 = 0.038 s at 3T and 0.032 s at 7T. For GAG, exchange rate = 1000 Hz, concentration = 0.3 M, T1 = 1 s, T2 = 0.01 s and chemical shift = 1 ppm.